

High-resolution 2D NMR spectra in inhomogeneous fields based on intermolecular multiple-quantum coherences with efficient acquisition schemes

Meijin Lin ^{a,b}, Yuqing Huang ^a, Xi Chen ^{a,*}, Shuhui Cai ^a, Zhong Chen ^{a,*}

^a Department of Physics, Fujian Key Laboratory of Plasma and Magnetic Resonance, State Key Laboratory of Physical Chemistry of Solid Surfaces, Xiamen University, Xiamen 361005, China

^b Department of Oceanography, Key Laboratory of Underwater Acoustic Communication and Marine Information Technology, Ministry of Education, Xiamen University, Xiamen 361005, China

ARTICLE INFO

Article history:

Received 26 August 2010

Revised 11 October 2010

Available online 16 October 2010

Keywords:

High-resolution

J-resolved spectroscopy

COSY

Efficient acquisition schemes

Intermolecular multiple-quantum coherences

Inhomogeneous fields

ABSTRACT

High-resolution 2D NMR spectra in inhomogeneous fields can be achieved by the use of intermolecular multiple-quantum coherences and shearing reconstruction of 3D data. However, the long acquisition time of 3D spectral data is generally unbearable for *in vivo* applications. To overcome this problem, two pulse sequences dubbed as iDH-COSY and iDH-*J*RES were proposed in this paper. Although 3D acquisition is still required for the new sequences, the high-resolution 2D spectra can be obtained with a relatively short scanning time utilizing the manipulation of indirect evolution period and sparse sampling. The intermolecular multiple-quantum coherence treatment combined with the raising and lowering operators was applied to derive analytical signal expressions for the new sequences. And the experimental observations agree with the theoretical predictions. Our results show that the new sequences possess bright perspective in the applications on *in vivo* localized NMR spectroscopy.

© 2010 Elsevier Inc. All rights reserved.

1. Introduction

Different kinds of techniques have been utilized to achieve high-resolution 1D NMR spectra in inhomogeneous fields, such as the algorithms based on image deconvolution [1], Fourier synthesis [2,3], nutation echo [4–6], intermolecular multiple-quantum coherences (iMQCs) [7], etc. In recent years, iMQCs have been proven to be a promising strategy in many case, such as for enhancement of contrast in magnetic resonance imaging [8–10], and high-resolution NMR spectra in inhomogeneous fields. The high-resolution iMQC spectroscopy uses 2D technique to average out inhomogeneous broadenings by correlating the iMQC transition with the conventional single-quantum coherence (SQC) one [7,11–15]. After a shearing process [11,15,16], a high-resolution 1D spectrum free of inhomogeneous broadenings can be extracted from the projection along one dimension of the acquired 2D spectrum while the information along the other dimension containing inhomogeneous broadenings are discarded. The high-resolution iMQC spectroscopy has been applied to the *in vivo* localized magnetic resonance spectroscopy (MRS) with field-distorted voxels, where the spectral linewidths are broadened by the magnetic field

gradients caused by susceptibility differences between tissues, bones and air [17–21].

2D MRS such as *J*-resolved spectroscopy (*J*-RES), COSY and multiple-quantum coherence spectroscopy has been applied to obtain more spectral information and better signal separation [22–25]. The methodology for quantification of metabolites *via* 2D MRS was also established and well applied [26,27]. However, in the presence of field distortions caused by susceptibility gradients, line broadenings occur in these 2D spectra, for the routine 2D MRS such as COSY and *J*-RES, both t_1 and t_2 periods are conventional SQC evolution. We have demonstrated that in above two kinds of spectra the tilt angles of the inhomogeneous broadenings and the chemical shift alignment (of diagonal peaks for the COSY case) orient at the same direction in the 2D spectra [28], resulting in the overlapping of adjacent resonances. Thus the metabolite quantification is seriously influenced. The inhomogeneous broadening effect also presents in the projection spectra of COSY and *J*-RES in one or two dimensions. In our recent work [29,30], we extended the concept of high-resolution iMQC MRS from 1D to 2D, taking the most common ones, COSY and *J*-RES, as examples.

In this paper, two pulse sequences, which are based on the intermolecular double-quantum filter HOMOGENIZED (iDH) sequence [13] and thus dubbed iDH-COSY and iDH-*J*RES, are proposed to shorten acquisition time of iMQC high-resolution COSY and *J*-RES spectra in inhomogeneous fields. For the new sequences, the three-dimensional (3D) iMQC approach is utilized to obtain 2D

* Corresponding authors. Fax: +86 592 2189426.

E-mail addresses: xichen.nmr@gmail.com (X. Chen), chenz@xmu.edu.cn (Z. Chen).

MRS free of inhomogeneous broadening effect. Similar to the 2D iMQC approach used to obtain 1D high-resolution MRS, one dimension of the 3D spectrum is discarded after shearing processes. The other two dimensions, which are almost free of inhomogeneous broadenings, can be utilized to achieve different coherences of 2D MRS and the transition between them. The time efficient acquisition scheme based on the reduction of one of the indirect spectral widths [15,16] is used to shorten the acquisition time without any sensitivity loss.

2. Theories and methods

The iDH-COSY and iDH-JRES pulse sequences are shown in Fig. 1a and b, respectively. Except for the second RF pulse and the manipulation of evolution periods, these two sequences are the same. Three linear coherence selection gradients (CSGs) are applied to select the following coherence transfer pathway for both sequences, $0 \rightarrow +2 \rightarrow +1 \rightarrow -1$. Since the 3D iMQC approach is required for the new sequences, two indirect evolution periods t_1 and t_2 are presented. The comparison of the two pulse sequences is shown in Table 1.

Without loss of generality, a homogeneous liquid mixture consisting of an AX spin-1/2 system of S component (including S_k and S_l spins with a scalar coupling constant J_{kl}) and a single spin-1/2 system of I component is considered. It is assumed that I spin (corresponding to solvent) is abundant and S spin (corresponding to solute) is either abundant or dilute. Assume that ω_m is the frequency offset of spin m ($m = I, S_k, S_l$) in the rotating frame in the absence of field inhomogeneity, and $\Delta B(\mathbf{r})$ is the field inhomogeneity at position \mathbf{r} . When spatially dependent magnetic field is taken into account, the frequency offset, $\Omega_m(\mathbf{r})$, of spin m at position \mathbf{r} is given by:

$$\Omega_m(\mathbf{r}) = \omega_m + \Delta\omega(\mathbf{r}) = \omega_m + \gamma \cdot \Delta B(\mathbf{r}), \quad (m = I, S_k, S_l), \quad (1)$$

where γ is the gyromagnetic ratio. Eq. (1) suggests that the magnetic field inhomogeneity causes a shift of angular frequency from the resonance ω_m . Since both evolution period t_1 and acquisition period t_2 are SQC evolutions for the conventional COSY [31] and J-RES [32] spectra, the spectral information provided by these two conventional approaches are demolished by magnetic field inhomogeneity. However, the new sequences, iDH-COSY and iDH-JRES, provide ways to eliminate the inhomogeneous broadenings in both F1 and F2 dimensions. In addition, since the distant dipolar field (DDF) originated from solvent has an equal effect on all solute spins with the same spatial distribution and does not affect the J coupling between solute spins, the COSY and J-RES spectral property and information are preserved.

2.1. iDH-COSY

The detailed theoretical derivation of the spin evolution under the iDH-COSY (Fig. 1a) is based on the iMQC treatment combined

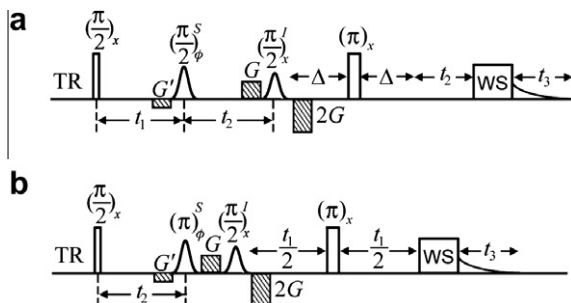


Fig. 1. High-resolution 2D MRS sequences via 3D iMQCs: (a) iDH-COSY and (b) iDH-JRES.

Table 1

Coherence orders and acquisition schemes of 3D iMQC pulse sequences.

Pulse sequence	Evolution period t_1	Mixing pulse	Evolution period t_2	Acquisition scheme on t_2
iDH-COSY	iZQC	2nd RF pulse ($\frac{\pi}{2}S_x$)	iDQC	Delay acquisition
iDH-JRES	Spin echo	N/A	iZQC	Fold-over correction

with the raising and lowering operators. For simplification, the effects of radiation damping, diffusion, relaxation, and intermolecular NOE are ignored, and the CSGs are applied along the z direction. For the iDH-COSY sequence, the first RF pulse $(\pi/2)_x$ rotates the equilibrium density operator into the transverse plane. After dropping unimportant factors and terms, we can use raising and lowering operators to express the double-quantum term $S_{ky}I_y$, excluding $S_{ky}S_{ly}$ term, in the reduced density operator as [33]

$$\sigma(0^+) = \sum_{i=1}^{N_I} \sum_{j=1}^{N_S} I_{yi} S_{kyj} = \frac{1}{4} \sum_{i=1}^{N_I} \sum_{j=1}^{N_S} \left[(I_i^+ S_{kj}^- + I_i^- S_{kj}^+) - (I_i^+ S_{kj}^+ + I_i^- S_{kj}^-) \right], \quad (2)$$

where I_{yi} represents the y component of the i th I spin operator, S_{kyj} represents the y component of the j th S_k spin operator, and N_I and N_S are the total molecule numbers of I and S spins, respectively. According to the coherence transfer pathway in the iDH-COSY, only the term $I_i^+ S_{kj}^-/4$ in Eq. (2) is chosen by the CSGs. Then, during the evolution period t_1 , we have

$$\sigma(t_1) = \frac{1}{4} \sum_{i=1}^{N_I} \sum_{j=1}^{N_S} I_i^+ [S_{kj}^- \cos(\pi J_{kl} t_1) + i2S_{kj}^- S_{lj}] \times \sin(\pi J_{kl} t_1) e^{-i[\varphi(r_i) - \varphi(r_j)]} e^{-i(\Omega_i - \Omega_{S_k}) t_1}. \quad (3)$$

The dephasing angles at positions r_i and r_j for I^+ and S^- due to the correlation gradient G' are $\varphi(r_i) = \gamma G' \delta z_i$ and $\varphi(r_j) = \gamma G' \delta z_j$, where z_i and z_j are the projections of the positions r_i and r_j along the z direction, respectively.

The solute-selective $(\pi/2)_\phi^S$ RF pulse (ϕ is the phase shift angle) implements the coherence transfer of S spin between the evolution periods t_1 and t_2 . After the $(\pi/2)_x^S$ RF pulse ($\phi = x$), the spin density operators evolve into the following terms: $I_i^+ S_{kj}^-/8$, $I_i^+ S_{kj}^+/8$, $-iI_i^+ S_{kz}/4$, $i2I_i^+ S_{kzj} S_{lj}^+/8$, $-i2I_i^+ S_{kzj} S_{lj}^-/8$, $-I_i^+ S_{kj}^+ S_{lj}^+/8$, $I_i^+ S_{kj}^+ S_{lj}^-/8$, $-I_i^+ S_{kj}^- S_{lj}^+/8$, and $I_i^+ S_{kj}^- S_{lj}^-/8$. Since the subsequent solvent-selective $(\pi/2)_x^I$ RF pulse and the related field gradients (G and $2G$) form a double-quantum filter (DQF), only the terms $I_i^+ S_{kj}^+/8$ and $i2I_i^+ S_{kzj} S_{lj}^+/8$ are preserved. These two terms evolve during the first t_2 evolution period. After that, the $(\pi/2)_x^I$ RF pulse transforms I^+ into $(0.5I^+ + 0.5I^- + iI_z)$. The fourth non-selective pulse $(\pi)_x$ is inserted in the middle of delay interval ($2A$) to prevent the dephasing of signals before the DDF takes effect. Since there are no subsequent pulses, we only need to consider the SQC terms that contribute to observable signals. Before the second t_2 evolution period, we have

$$\sigma(t_1 + 2t_2) = \frac{1}{8} \sum_{i=1}^{N_I} \sum_{j=1}^{N_S} \left\{ -I_z [iS_{kj}^- \cos(\pi J_{kl} t_1) \cos(\pi J_{kl} t_2) + 2S_{kj}^- S_{lj} \cos(\pi J_{kl} t_1) \sin(\pi J_{kl} t_2)] \times e^{-i[\varphi(r_i) - \varphi(r_j) + \varphi_1(r_i) - \varphi_1(r_j)]} e^{-i(\Omega_i - \Omega_{S_k}) t_1 + (\Omega_{S_k} + \Omega_l) t_2} - I_z [iS_{lj}^- \sin(\pi J_{kl} t_1) \sin(\pi J_{kl} t_2) - 2S_{kzj} S_{lj}^- \sin(\pi J_{kl} t_1) \cos(\pi J_{kl} t_2)] \times e^{-i[\varphi(r_i) - \varphi(r_j) + \varphi_1(r_i) - \varphi_1(r_j)]} \times e^{-i(\Omega_i - \Omega_{S_k}) t_1 + (\Omega_{S_k} + \Omega_l) t_2} \right\}. \quad (4)$$

$\varphi_1(r_i) = \gamma G \delta z_i$ and $\varphi_1(r_j) = \gamma G \delta z_j$ are the dephasing angles at positions r_i and r_j for I^+ and S^+ due to the field gradient G , respectively.

Since the module of excitation sculpting (WS) right before acquisition only acts to suppress the solvent signals and does not influence the desired solute signals, we ignore it in the following deduction. The observable signal at the detection period can be written as

$$\begin{aligned} \sigma(t_1 + 2t_2 + t_3) = & \frac{-i\pi(t_2 + t_3)}{16} \sum_{j=1}^{N_s} \left\{ S_{kj}^- e^{-i[(\Omega_l - \Omega_{S_k})t_1 + \Omega_l t_2 - \Omega_{S_k} t_3]} \cos(\pi J_{kl} t_1) \right. \\ & \times \cos[\pi J_{kl}(2t_2 + t_3)] \sum_{i=1}^{N_l} D_{ij} e^{-i\gamma\delta(G+G')(z_i - z_j)} \\ & + S_{ij}^- e^{i[(\Omega_l - \Omega_{S_k})t_1 + \Omega_l t_2 - \Omega_{S_k} t_3]} \sin(\pi J_{kl} t_1) \times \sin[\pi J_{kl}(2t_2 + t_3)] \\ & \left. \times \sum_{i=1}^{N_l} D_{ij} e^{-i\gamma\delta(G+G')(z_i - z_j)} \right\}. \end{aligned} \quad (5)$$

where D_{ij} is the residual intermolecular dipolar coupling constant. Since we are free to choose the origin of the coordinate system, we can set $z_j = 0$, hence

$$\sum_{i=1}^{N_l} D_{ij} e^{-i\gamma\delta(G+G')(z_i - z_j)} = \sum_{i=1}^{N_l} D_{ij} \left\{ \cos[\gamma(G+G')\delta z_i] - i \sin[\gamma(G+G')\delta z_i] \right\}. \quad (6)$$

Summation over dipolar-coupled spins can be replaced by an integral if the distribution of the spins can be considered continuous. Since sine is an odd function, the term containing $\sin[\gamma(G+G')\delta z_i]$ in Eq. (6) vanishes when the sum over the sample is performed. After the spatial integral over the whole sample volume is performed, we have

$$\begin{aligned} \sigma(t_1 + 2t_2 + t_3) = & \frac{-i\pi(t_2 + t_3)\Delta_s}{24\tau_d^l} \left(\frac{kT}{\hbar\omega_l} \right) \sum_{j=1}^{N_s} \left\{ S_{kj}^- e^{-i[(\Omega_l - \Omega_{S_k})t_1 + \Omega_l t_2 - \Omega_{S_k} t_3]} \right. \\ & \times \cos(\pi J_{kl} t_1) \times \cos[\pi J_{kl}(2t_2 + t_3)] \\ & + S_{ij}^- e^{-i[(\Omega_l - \Omega_{S_k})t_1 + \Omega_l t_2 - \Omega_{S_k} t_3]} \sin(\pi J_{kl} t_1) \\ & \left. \times \sin[\pi J_{kl}(2t_2 + t_3)] \right\}. \end{aligned} \quad (7)$$

where $\Delta_s = [3(\hat{s} \cdot \hat{z})^2 - 1]/2$, \hat{s} and \hat{z} represent unit vectors along the directions of field gradient and static magnetic field, respectively, $(\hbar\omega_l/kT)$ is the Boltzmann factor, and the dipolar demagnetizing time $\tau_d^l = 1/(\mu_0\gamma M_0^l)$, in which M_0^l is the equilibrium magnetization per unit volume of l spin. Thus the observable signal $M_{\pm}^{S_k}$ can be calculated to be

$$\begin{aligned} M_{\pm}^{S_k}(t_1 + 2t_2 + t_3) = & \text{Tr}[\sigma(t_1 + 2t_2 + t_3)\gamma\hbar(S_k^+ + S_l^+)/V] \\ = & \frac{-i\pi M_0^S(t_2 + t_3)\Delta_s}{6\tau_d^l} \left\{ e^{-i[(\Omega_l - \Omega_{S_k})t_1 + \Omega_l t_2 - \Omega_{S_k} t_3]} \cos(\pi J_{kl} t_1) \right. \\ & \times \cos[\pi J_{kl}(2t_2 + t_3)] + e^{-i[(\Omega_l - \Omega_{S_k})t_1 + \Omega_l t_2 - \Omega_{S_k} t_3]} \\ & \left. \times \sin(\pi J_{kl} t_1) \sin[\pi J_{kl}(2t_2 + t_3)] \right\}, \end{aligned} \quad (8)$$

where M_0^S is the equilibrium magnetization per unit volume of S spin. From Eq. (8), we notice that this iMQC signal evolves at $(\Omega_{S_k} - \Omega_l)$ and Ω_l during the evolution period t_1 and t_2 , respectively. For the iMQCs, $(\Omega_{S_k} - \Omega_l)$ is the difference frequency between solvent and solute spins at the correlation distance apart, which is typically around 10–100 μm and much smaller than the macroscopic spatial variations of static magnetic field. Hence, $\Delta B_l(r) \approx \Delta B_s(r)$ and the difference frequency $(\Omega_{S_{kl(l)}} - \Omega_l)$ can be approximated by $(\omega_{S_{kl(l)}} - \omega_l)$, which suggests that the inhomogeneity is eliminated within the correlation distance for the iMQC signals. Then Eq. (8) can be rearranged to

$$\begin{aligned} M_{\pm}^{S_k}(t_1, 2t_2, t_3) = & \frac{-i\pi M_0^S(t_2 + t_3)\Delta_s}{24\tau_d^l} \left\{ e^{i[(\omega_{S_k} + \pi J_{kl} - \omega_l)t_1 + (-\Omega_l + 2\pi J_{kl})t_2 + (\Omega_{S_k} + \pi J_{kl})t_3]} \right. \\ & + e^{i[(\omega_{S_k} + \pi J_{kl} - \omega_l)t_1 + (-\Omega_l - 2\pi J_{kl})t_2 + (\Omega_{S_k} - \pi J_{kl})t_3]} \\ & + e^{i[(\omega_{S_k} - \pi J_{kl} - \omega_l)t_1 + (-\Omega_l + 2\pi J_{kl})t_2 + (\Omega_{S_k} + \pi J_{kl})t_3]} \\ & + e^{i[(\omega_{S_k} - \pi J_{kl} - \omega_l)t_1 + (-\Omega_l - 2\pi J_{kl})t_2 + (\Omega_{S_k} - \pi J_{kl})t_3]} \\ & - e^{i[(\omega_{S_k} + \pi J_{kl} - \omega_l)t_1 + (-\Omega_l + 2\pi J_{kl})t_2 + (\Omega_{S_k} + \pi J_{kl})t_3]} \\ & + e^{i[(\omega_{S_k} + \pi J_{kl} - \omega_l)t_1 + (-\Omega_l - 2\pi J_{kl})t_2 + (\Omega_{S_k} - \pi J_{kl})t_3]} \\ & + e^{i[(\omega_{S_k} - \pi J_{kl} - \omega_l)t_1 + (-\Omega_l + 2\pi J_{kl})t_2 + (\Omega_{S_k} + \pi J_{kl})t_3]} \\ & \left. - e^{i[(\omega_{S_k} - \pi J_{kl} - \omega_l)t_1 + (-\Omega_l - 2\pi J_{kl})t_2 + (\Omega_{S_k} - \pi J_{kl})t_3]} \right\}. \end{aligned} \quad (9)$$

Eq. (9) provides a quantitative expression of the diagonal and cross peaks in 3D iDH-COSY spectrum for the S_k spin. It includes eight terms due to J coupling and coherence transfers. The first four terms represent the diagonal peak for the S_k spin, whose locations are $(\Omega_1, \Omega_2, \Omega_3) = [-(\omega_{S_k} \pm \pi J_{kl} - \omega_l), -(\Omega_l \pm 2\pi J_{kl}), \Omega_{S_k} \pm \pi J_{kl}]$. The last four terms represent the cross peak between S_k and S_l spins, whose locations are $(\Omega_1, \Omega_2, \Omega_3) = [-(\omega_{S_k} \pm \pi J_{kl} - \omega_l), -(\Omega_l \pm 2\pi J_{kl}), \Omega_{S_l} \pm \pi J_{kl}]$. It can be seen that the F2 dimension only contains the frequency of the solvent ω_l and the broadenings caused by the inhomogeneous fields. That means the sampling rate of the F2 dimension can be reduced to a bit larger than the inhomogeneous broadened linewidth, which is ca. 0.1 ppm or smaller for *in vivo* detections. Assuming a reduced sampling rate for a spectral width of 0.2 ppm instead of 10 ppm, the scanning efficiency can be improved by as much as 50 times.

Because the inhomogeneous broadening in the expression of $e^{i(\Omega_l \pm 2\pi J_{kl})t_2}$ in Eq. (9) is along the F2 dimension (see Fig. 2a), a shearing process of the F2–F3 plane along the F3 axis is required to obtain high-resolution projection on the F3 axis: $\Omega'_3 = \Omega_3 - \Omega_2 = \omega_{S_{kl(l)}} \pm 3\pi J_{kl} - \omega_l$, which transforms the location of peaks into $(\Omega_1, \Omega_2, \Omega'_3) = [-(\omega_{S_k} \pm \pi J_{kl} - \omega_l), -(\Omega_l \pm 2\pi J_{kl}), \omega_{S_{kl(l)}} \pm 3\pi J_{kl} - \omega_l]$. (10)

Therefore, the F3 dimension is no longer suffered from inhomogeneous broadening effect (Fig. 2b). A high-resolution COSY spectrum can be extracted by projecting the 3D spectrum onto the F1–F3 plane. In addition, the J coupling constants in the F1 dimension are kept unchanged while those in the F3 dimension are magnified by a factor of 3, which would be useful for the spin systems with small J coupling constants.

2.2. iDH-JRES

The iDH-JRES sequence shown in Fig. 1b is quite similar to the iDH-COSY sequence in the pulse arrangement but changes the second RF pulse from π to $\pi/2$ since there is no coherence transfer in the J -RES. The major difference between these two sequences is the manipulation of the evolution periods. The spin echo period in the iDH-JRES sequence is used as the first evolution period, which is the same as that in conventional J -resolved sequence and insensitive to inhomogeneous fields. In addition, the iZQC period is used as the second evolution period of the iDH-JRES sequence, equivalent to the chemical shift dimension of the conventional one.

Similar deduction can be performed for the iDH-JRES sequence to obtain the theoretical expression. The quantitative expression of the signals in 3D iDH-JRES spectrum for the S_k spin can be expressed as

$$\begin{aligned} M_{\pm}^{S_k}(t_1, t_2, t_3) = & \frac{-i\pi M_0^S(0.5t_2 + t_3)\Delta_s}{3\tau_d^l} \left\{ e^{i[(\omega_{S_k} + \pi J_{kl} - \omega_l)t_2 + \pi J_{kl} t_1 + (\Omega_{S_k} + \pi J_{kl})t_3]} \right. \\ & \left. + e^{i[(\omega_{S_k} - \pi J_{kl} - \omega_l)t_2 - \pi J_{kl} t_1 + (\Omega_{S_k} - \pi J_{kl})t_3]} \right\}, \end{aligned} \quad (11)$$

which indicates that the peaks are at $(\Omega_1, \Omega_2, \Omega_3) = [\mp\pi J_{kl}, -(\omega_{S_k} \pm \pi J_{kl} - \omega_l), \Omega_{S_k} \pm \pi J_{kl}]$. Compared to the SQCs in the

conventional J -RES, the iZQC signal in t_2 period of the iDH-JRES is free of inhomogeneous broadening, thus a high-resolution chemical shift dimension can be achieved. In addition, only J -coupling information is preserved in the t_1 period of the iDH-JRES, the spectral pattern of J -RES is therefore achieved.

Since there is no coherence transfer of solute spins between the t_2 and t_3 periods, there are only diagonal peaks aligning in a narrow band of the F2–F3 plane. Similar to the high-resolution COSY, the efficient acquisition scheme by reducing the sampling spectral width of one indirect dimension can also be applied for the iDH-JRES. The fold-over correction (FOC) scheme, which has been used to speed up the acquisition of iZQC spectroscopy, is suitable for efficiently sampling the F2–F3 plane of the 3D iMQC data. Assume the frequency offsets are Ω_2 and Ω_3 in the F2 and F3 dimensions,

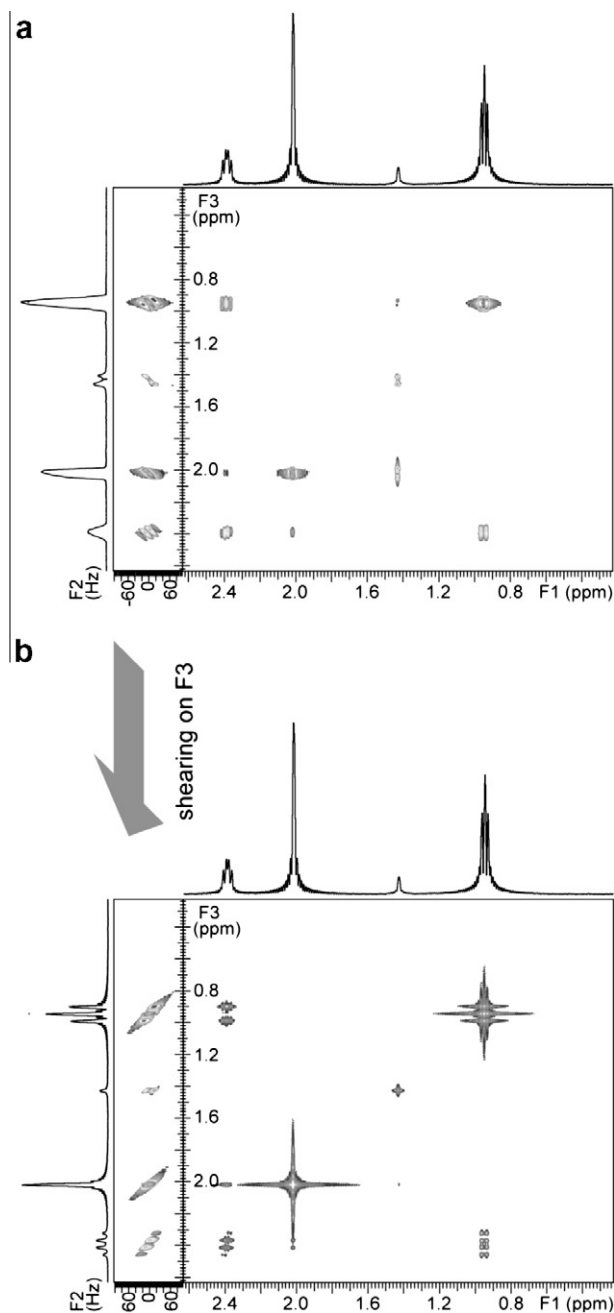


Fig. 2. Shearing process for iDH-COSY: the spectra before (a) and after (b) shearing along F2 dimension.

respectively. Folding in the F2 dimension of a spectrum occurs if Ω_2 exceeds the Nyquist frequency ω_2^N . Folding leads Ω_2 to an apparent frequency:

$$\Omega_2^F = [(\Omega_2 + \omega_2^N) \bmod (2\omega_2^N)] - \omega_2^N, \quad (12)$$

where mod is the modulo operator for finding the remainder of division of the former by the latter (see Fig. 3a). If the spectral width in F2 is sufficient to cover the width of the frequency band, FOC can untangle the folded spectrum by shearing the experimental matrix Ω_2^F into Ω_2^{FOC} :

$$\Omega_2^{\text{FOC}} = [(\Omega_2^F + \Omega_3 + \omega_2^N) \bmod (2\omega_2^N)] - \omega_2^N. \quad (13)$$

The resulting spectrum is equivalent to the fully-sampled spectrum after a shearing along the F2 dimension: $(\Omega_2^{\text{FOC}}, \Omega_3) = (\Omega_2 + \Omega_3, \Omega_3)$. Therefore, after the FOC, the location of peaks in Eq. (11) on F2 axis is changed to $\Omega_2^{\text{FOC}} = \Omega_2 + \Omega_3 = \Omega_l$ (Fig. 3b). Since FOC results in inhomogeneous broadenings along the F2 axis, the 2nd shearing process along the F3 dimension in the F2–F3 plane is required, which converts the location of peaks on F3 axis to $\Omega_3' = \Omega_3 - \Omega_2^{\text{FOC}} = \omega_{s_k} - \omega_l$ (Fig. 3c).

After the above shearing, the signals are located at $(\Omega_l, \Omega_2^{\text{FOC}}, \Omega_3') = (\mp\pi J_{kl}, \Omega_l, \omega_{s_k} - \omega_l)$. A high-resolution projection spectrum without inhomogeneous line broadenings can be obtained in the F3 dimension. Compared to the delay acquisition scheme, there is no scaling for the J coupling constants. Finally, an iDH-JRES

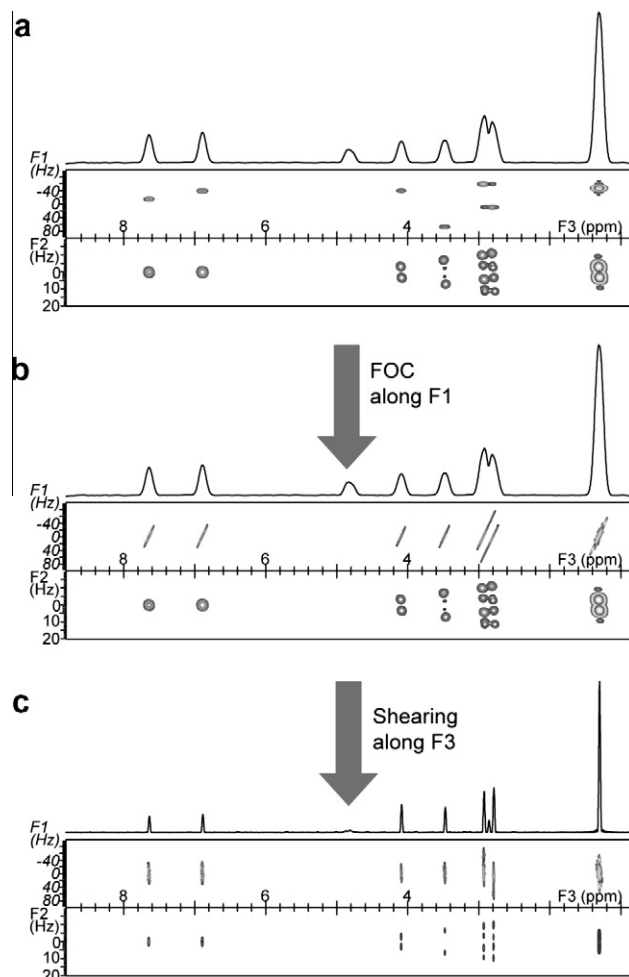


Fig. 3. Shearing process of iDH-JRES: the raw spectrum (a), the spectra after shearing with fold-over correction along the F1 dimension (b) and after shearing along the F3 dimension (c).

spectrum free of inhomogeneity can be extracted from the projection of the 3D iMQC data onto the F1–F3 plane. Table 2 shows the comparison of properties of several 2D NMR spectra.

3. Experimental

All experiments were performed on an 11.74 T Varian NMR System equipped with a 5 mm ^1H $\{^{15}\text{N}$ – $^{31}\text{P}\}$ XYZ indirect detection probe with 3D gradient coils. Two solution phantoms were used to demonstrate implementation details of the new sequences. Phantom I is a solution of butanone in cyclohexane with a molar ratio of 1:1000, and Phantom II is an aqueous solution of 10 mM histidine (His) and 10 mM lactate (Lac). The Z1 shimming coil was deliberately detuned to produce a linewidth of 50 Hz to simulate the static field inhomogeneity. The schematics of the new pulse sequences are presented in Fig. 1. The excitation sculpting scheme [34] of two frequency selective refocusing pulses was applied as the water suppression (WS) module. The W5 composite pulse [35] was used for the water-exclusive π pulse right before the intermolecular DQF period and the two water-exclusive π pulses in the WS module. The parameters (strength \times duration) of gradients were $G' = 0.07 \text{ T/m} \times 1.2 \text{ ms}$, $G = 0.16 \text{ T/m} \times 1.2 \text{ ms}$, $G_1 = 0.14 \text{ T/m} \times 1.0 \text{ ms}$, and $G_2 = 0.24 \text{ T/m} \times 1.0 \text{ ms}$, respectively, where G_1 and G_2 are the spoiling pulse field gradients in the WS module. A 2-step phase cycling was applied: $\phi = (x, y)$ and receiver = $(x, -x)$. Phantom I was used for the COSY measurements. The

repetition time (TR) and the echo time (TE) were TR/TE = 1000/100 ms. $192 \times 16 \times 300$ points were acquired with spectral widths of $1200 \times 100 \times 1200 \text{ Hz}$ ($F1 \times F2 \times F3$) in 2 h. Conventional J -RES and the iDH- J -RES via 3D iMQCs were applied on Phantom II. $12 \times 10 \times 256$ points were acquired with spectral widths of $100 \times 50 \times 4000 \text{ Hz}$ ($F1 \times F2 \times F3$) in 20 min. The average number of transients of each t_1 increment was 4 and TR/TE = 2000 ms/40 ms.

4. Results and discussion

4.1. Results for the COSY

The COSY spectra obtained with different pulse sequences are presented in Fig. 4. The phantom I was used for these studies. The solvent, cyclohexane, was suppressed in these experiments. The conventional COSY spectrum is shown in Fig. 4a. The inhomogeneous field results in line broadenings stretching along the diagonal direction of the 2D spectrum. The coherence orders of the conventional COSY are +1 and –1 in t_1 and t_2 periods, respectively, by which the broadening direction of the peaks in the 2D spectrum is determined. Since the evolutions in both t_1 and t_2 periods are sensitive to inhomogeneous fields, the 1D projection spectra along both F1 and F2 dimensions are suffered from inhomogeneous broadenings. The J coupling multiplets are hardly resolved in either the 1D projection spectra or the 2D spectrum. Furthermore, it is

Table 2
2D spectral properties of typical 2D sequences and new 3D iMQC sequences in inhomogeneous fields.

Pulse sequence	Inhomogeneous broadening direction	Chemical shift direction	Scale of J multiplet in F1 dimension	Scale of J multiplet in F2 dimension	References
COSY	Diagonal	Diagonal	Unresolved	Unresolved	[31]
HOMOGENIZED	F2	Diagonal	1 Time	Unresolved	[7]
iDH-COSY	F3	Diagonal	1 Time	3 Times	This work
J -RES	F2	F2	1 Time	Unresolved	[32]
iDH- J -RES	F3	F2	1 Time	Decoupled	This work

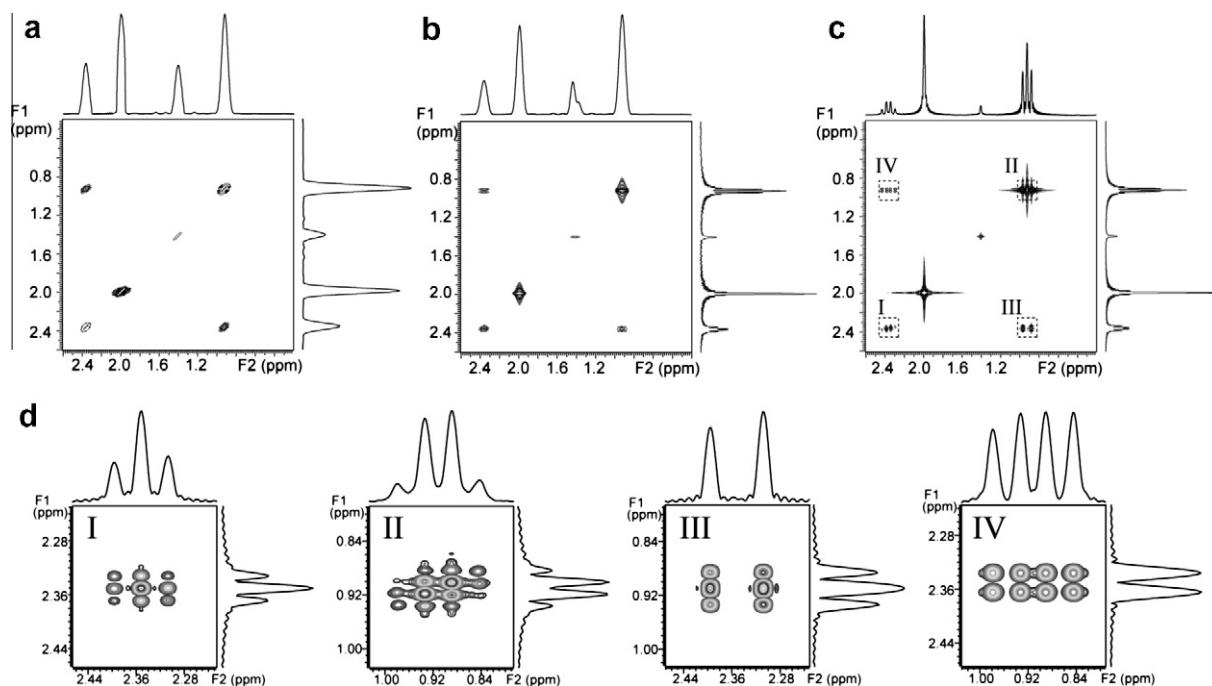


Fig. 4. COSY spectra obtained via (a) conventional 2D COSY sequence, (b) HOMOGENIZED sequence, and (c) the projection of 3D iMQC spectrum with the expanded multiplets in (d). The sample is a solution of butanone in cyclohexane with a molar ratio of 1:1000.

known that the chemical shift alignment of the diagonal peaks is along the diagonal direction, which is the same as the direction of the inhomogeneous broadened peaks stretching along. Therefore, the inhomogeneous broadenings may result in the overlapping of neighboring diagonal peaks in the 2D spectrum. The COSY spectrum obtained from the HOMOGENIZED sequence [7] was presented in Fig. 4b. Since the iZQC evolution period is insensitive to the inhomogeneous field, a high-resolution projection spectrum can be obtained in the indirect dimension. The problem of the overlapping caused by the inhomogeneous broadened diagonal peaks can be avoided since the stretching lines are no longer along the diagonal direction but parallel to the F2 axis instead. However, the evolution in the t_2 period is still subject to dephasing caused by the inhomogeneous field. The broadening in the F2 dimension greatly reduces the spectral resolution thus hinders the J scaling multiplets from being resolved. It may also lead to the overlapping of neighboring diagonal and cross peaks in the 2D spectrum.

The line broadenings in the F2 dimension can be removed by replacing SQCs with iMQCs. The 3D iMQC spectroscopy is utilized to achieve this aim and the result is demonstrated in Fig. 4c. Similar to Fig. 4b, the iZQC evolution period achieves high-resolution in the F1 dimension. On the other hand, the iDQC with the delay acquisition scheme is utilized in the t_2 period of Fig. 4c. The F3 dimension (not displayed in Fig. 4c) is the direct detection dimension. After the shearing process of the F2–F3 plane, a high-resolution spectrum free of inhomogeneous line broadening can be achieved in the F2 dimension, while the F3 dimension can be discarded by projecting the 3D data onto the F1–F2 plane. The projection is an accumulation projection. As a result, a high-resolution spectrum is achieved in both dimensions of the F1–F2 projection spectrum. Both chemical shift information and J multiplet patterns are preserved and the peak overlapping is avoided. Since iDQC is used in the t_2 period, a three-time magnification of J coupling constants is obtained in the F2 dimension, which favors the detection of weakly-coupled spin systems but hinders that of strongly-coupled ones.

4.2. Results for the J -RES

The comparison between conventional and high-resolution J -RES spectra under inhomogeneous fields is presented in Fig. 5. The phantom II is used. Fig. 5a is the conventional J -RES spectrum. Since the inhomogeneous broadening is refocused in the t_1 period by spin echo, the broadened lines stretch along the F2 axis. As a result, though the inhomogeneous line broadening is eliminated in the F1 dimension, the F2 dimension is still subject to inhomogeneous line broadening. Since the linewidth caused by the inhomogeneous broadening is generally much larger than J coupling constants, the J homo-decoupled spectrum extracted from the projection along the F2 axis can hardly achieve higher resolution for better quantification than conventional 1D spectrum. Furthermore, the 2D spectral information is also influenced by the inhomogeneous broadening since the chemical shifts of different resonances align along the F2 axis. Therefore, the broadened lines may cause the overlapping of resonances with close frequencies. In Fig. 5a, the α and β -proton resonances of His overlap to some degree. Also, the strongly-coupled artifacts between them can hardly be observed due to the overlapping caused by inhomogeneous broadening (see Fig. 5a inset). Similar to the iDH-COSY, a solution to this problem is replacing the SQC in the detection period by iMQCs. In Fig. 5b, iZQC is utilized in the t_2 period, and an efficient acquisition of this dimension is achieved by FOC. It can be seen from Fig. 5b that a much higher resolution in the F2 dimension can be obtained. The two quadruplets of His are well separated and the strongly-coupled resonance can be clearly observed in the

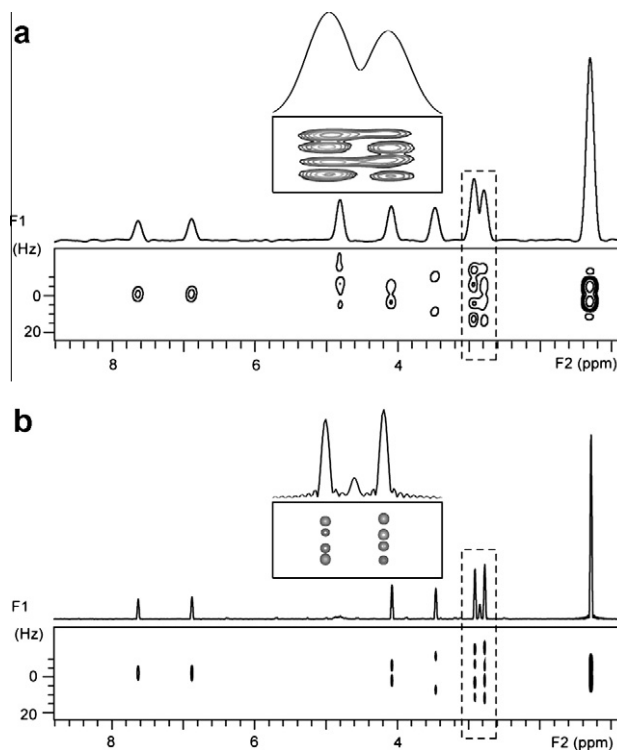


Fig. 5. J -RES spectra obtained via (a) conventional 2D J -RES sequence and (b) the projection of 3D iMQC spectrum. The sample is an aqueous solution of 10 mM His and 10 mM Lac.

projection spectrum (Fig. 5b inset). Better metabolite quantification via the J -decoupled projection spectrum can be achieved.

Furthermore, J modulations are greatly suppressed in the iDH- J -RES spectrum. Fig. 6a demonstrates severe integral ratio distortions in the original iZQC spectra with different TEs. The theoretical ratio of the seven peaks is 1:1:1:1:1:1:3. The iDH- J -RES spectrum (Fig. 6b) largely alleviates this problem and has similar integral ratio with the conventional spectrum with short TE (10 ms) under ideal shimming condition (Fig. 6c). It is because the iDH- J -RES is actually the combination of iZQC spectra with different TEs. As a result, J modulations are averaged and correct integral ratio is restored. The slight integral ratio distortion in both Fig. 6b and c may result from the influence of the water suppression.

4.3. Discussion

The sensitivity is a critical issue to iMQC high-resolution methods. It can be seen in Eq. (8) that the sensitivity of the iMQC high-resolution experiment relative to a conventional SQC experiment in a perfectly homogeneous field is affected by the concentration of solvent. For water solvent, the iMQC signal intensity is less than 10% of conventional SQC signal [16]. The sensitivity loss is a major drawback of the iMQC high-resolution methods in potential applications such as *in vivo* MRS. It is a trade-off for the improvement of spectral resolution under inhomogeneous fields. Also, it has been demonstrated that the sensitivity of high-resolution iMQC spectroscopy is hardly affected by the inhomogeneity under small to moderate inhomogeneous fields (inhomogeneity <1.2 ppm) [16,36]. Several techniques such as dynamic nuclear polarization technique [10,37] have been utilized for iMQC signal intensity improvement.

According to our experiments, the inhomogeneity of several ppm can be handled by the iMQC high-resolution methods on a 500 MHz spectrometer. It has been reported that the iMQC

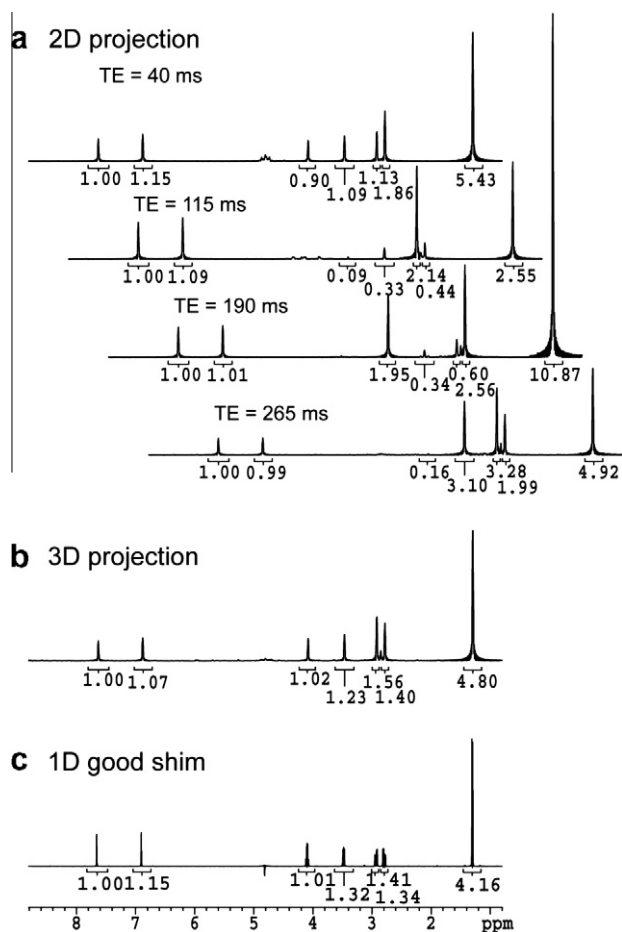


Fig. 6. Comparison of peak integral ratios: (a) homo-decoupled iZQC projection spectra with different TEs, (b) homo-decoupled projection spectrum of iDH-JRES, and (c) 1D conventional spectrum with WATERGATE under well-shimmed field (TE = 10 ms). All the integral values are normalized to the His peak at 7.8 ppm.

sequence can reduce the spectral linewidth from 7 ppm to 0.074 ppm under a severely distorted magnetic field [38]. However, as mentioned above, the bandwidth of the extra dimension of iDH-COSY and iDH-JRES should be larger than the field inhomogeneity to avoid fold-over, therefore the acquisition efficiency reduces as the magnetic field homogeneity deteriorates. The linewidths of iMQC high-resolution spectra mainly depend on the field inhomogeneity within the dipolar correlation distance. It has been shown that the iMQC spectral linewidth increases with the reduction of dipolar correlation distance under moderate inhomogeneous fields (with inhomogeneity of 0.5–1.3 ppm) [39].

5. Conclusions

In current work, high-resolution 2D MRS can be obtained in inhomogeneous fields via 3D iMQC acquisition scheme. The theoretical description is mainly focused on the elimination of inhomogeneous broadenings in both F1 and F2 dimensions with the original 2D spectral patterns preserved. In addition, time efficient acquisition schemes are applied to shorten the long acquisition time of 3D spectral data. To demonstrate the feasibility of the new sequences, some primary results on solution phantoms are presented. It can be seen that high-resolution spectra free of inhomogeneous broadenings are achieved in both dimensions of the 2D projection spectra, therefore the spectral information concealed by the inhomogeneous broadenings can be recovered, from

which the quantification of metabolite concentration may benefit. For iMQC high-resolution approaches, the spectral resolution is improved at the cost of scanning efficiency. Even with the efficient acquisition method presented in current work, the scanning time of a 3D iMQC spectroscopy is still lengthened by ca. 10 times compared to the conventional methods, which greatly reduce the applicability of the proposed methods. Some other acquisition schemes for sampling multidimensional data, such as Hardmand spectroscopy [40–42], *k*-space strategy [43,44] or compressed sensing [45,46], may be further utilized in corporation with the fast acquisition method used in this work.

Acknowledgments

This work was partially supported by the NNSF of China under Grants (10774125 and 10974164), and the Research Fund for the Doctoral Program of Higher Education of China under Grant 200803840019.

References

- [1] M.E. Halse, P.T. Callaghan, Imaged deconvolution: a method for extracting high-resolution NMR spectra from inhomogeneous fields, *J. Magn. Reson.* 185 (2007) 130–137.
- [2] B. Pryor, N. Khaneja, Fourier decompositions and pulse sequence design algorithms for nuclear magnetic resonance in inhomogeneous fields, *J. Chem. Phys.* 125 (2006) 194111.
- [3] H. Arthanari, D. Frueh, G. Wagner, B. Pryor, N. Khaneja, Fourier synthesis techniques for NMR spectroscopy in inhomogeneous fields, *J. Chem. Phys.* 128 (2008) 214503.
- [4] D. Sakellariou, C.A. Meriles, A. Moule, A. Pines, Variable rotation composite pulses for high resolution nuclear magnetic resonance using inhomogeneous magnetic and radiofrequency fields, *Chem. Phys. Lett.* 363 (2002) 25–33.
- [5] D. Sakellariou, S.P. Brown, A. Lesage, S. Hediger, M. Bardet, C.A. Meriles, A. Pines, L. Emsley, High-resolution NMR correlation spectra of disordered solids, *J. Am. Chem. Soc.* 125 (2003) 4376–4380.
- [6] D. Sakellariou, C.A. Meriles, A. Pines, Advances in *ex-situ* nuclear magnetic resonance, *CR Phys.* 5 (2004) 337–347.
- [7] S. Vathyam, S. Lee, W.S. Warren, Homogeneous NMR spectra in inhomogeneous fields, *Science* 272 (1996) 92–96.
- [8] U. Eliav, G. Navon, Enhancement of magnetization transfer effects by intermolecular multiple quantum filtered NMR, *J. Magn. Reson.* 190 (2008) 149–153.
- [9] W. Ling, U. Eliav, G. Navon, A. Jerschow, Chemical exchange saturation transfer by intermolecular double-quantum coherence, *J. Magn. Reson.* 194 (2008) 29–32.
- [10] M. Mishkovsky, U. Eliav, G. Navon, L. Frydman, Nearly 10^6 -fold enhancements in intermolecular ^1H double-quantum NMR experiments by nuclear hyperpolarization, *J. Magn. Reson.* 200 (2009) 142–146.
- [11] Z. Chen, Z.W. Chen, J.H. Zhong, High-resolution NMR spectra in inhomogeneous fields via IDEAL (intermolecular dipolar-interaction enhanced all lines) method, *J. Am. Chem. Soc.* 126 (2004) 446–447.
- [12] D. Balla, C. Faber, Solvent suppression in liquid state NMR with selective intermolecular zero-quantum coherences, *Chem. Phys. Lett.* 393 (2004) 464–469.
- [13] X. Chen, M.J. Lin, Z. Chen, S.H. Cai, J.H. Zhong, High-resolution intermolecular zero-quantum coherence spectroscopy under inhomogeneous fields with effective solvent suppression, *Phys. Chem. Phys.* 9 (2007) 6231–6240.
- [14] Z. Chen, T. Hou, Z.W. Chen, D.W. Hwang, L.P. Hwang, Selective intermolecular zero-quantum coherence in high-resolution NMR under inhomogeneous fields, *Chem. Phys. Lett.* 386 (2004) 200–205.
- [15] Z. Chen, S.H. Cai, Z.W. Chen, J.H. Zhong, Fast acquisition of high-resolution NMR spectra in inhomogeneous fields via intermolecular double-quantum coherences, *J. Chem. Phys.* 130 (2009) 084504.
- [16] X. Chen, M.J. Lin, Z. Chen, J.H. Zhong, Fast acquisition scheme for achieving high-resolution MRS with J-scaling under inhomogeneous fields, *Magn. Reson. Med.* 61 (2009) 775–784.
- [17] C. Faber, E. Pracht, A. Haase, Resolution enhancement in *in vivo* NMR spectroscopy: detection of intermolecular zero-quantum coherences, *J. Magn. Reson.* 161 (2003) 265–274.
- [18] D.Z. Balla, G. Melkus, C. Faber, Spatially localized intermolecular zero-quantum coherence spectroscopy for *in vivo* applications, *Magn. Reson. Med.* 56 (2006) 745–753.
- [19] D.Z. Balla, C. Faber, *In vivo* intermolecular zero-quantum coherence MR spectroscopy in the rat spinal cord at 17.6 T: a feasibility study, *Magn. Reson. Mater. Phys. Biol. Med.* 20 (2007) 183–191.
- [20] C. Faber, Resolution enhancement in *in vivo* NMR spectroscopy, *Annu. Rep. NMR Spectrosc.* 61 (2007) 1–50.
- [21] D.Z. Balla, C. Faber, Localized intermolecular zero-quantum coherence spectroscopy *in vivo*, *Concepts Magn. Reson. Part A* 32A (2008) 117–133.

- [22] L.N. Ryner, J.A. Sorenson, M.A. Thomas, Localized 2D J -resolved ^1H NMR spectroscopy: strong coupling effects *in vitro* and *in vivo*, *Magn. Reson. Imag.* 13 (1995) 853–869.
- [23] L.N. Ryner, J.A. Sorenson, M.A. Thomas, 3D Localized 2D NMR-spectroscopy on an MRI scanner, *J. Magn. Reson. Ser. B* 107 (1995) 126–137.
- [24] W. Dreher, D. Leibfritz, Detection of homonuclear decoupled *in vivo* proton NMR spectra using constant time chemical shift encoding: CT-PRESS, *Magn. Reson. Imag.* 17 (1999) 141–150.
- [25] R.A. de Graaf, D.L. Rothman, K.L. Behar, High resolution NMR spectroscopy of rat brain *in vivo* through indirect zero-quantum-coherence detection, *J. Magn. Reson.* 187 (2007) 320–326.
- [26] T. Lange, R.F. Schulte, P. Boesiger, Quantitative J -resolved prostate spectroscopy using two-dimensional prior-knowledge fitting, *Magn. Reson. Med.* 59 (2008) 966–972.
- [27] J.E. Jensen, S.C. Licata, D. Ongur, S.D. Friedman, A.P. Prescott, M.E. Henry, P.F. Renshaw, Quantification of J -resolved proton spectra in two-dimensions with LCMODEL using GAMMA-simulated basis sets at 4 Tesla, *NMR Biomed.* 22 (2009) 762–769.
- [28] Z. Chen, M.J. Lin, X. Chen, S.H. Cai, Advances in high-resolution nuclear magnetic resonance methods in inhomogeneous magnetic fields using intermolecular multiple quantum coherences, *Sci. China Ser. G – Phys. Mech. Astron.* 52 (2009) 58–69.
- [29] Y.Q. Huang, S.H. Cai, Y.Q. Lin, Z. Chen, An intermolecular single-quantum coherence detection scheme for high-resolution two-dimensional J -resolved spectroscopy in inhomogeneous fields, *Appl. Spectrosc.* 64 (2010) 235–240.
- [30] Y.Q. Huang, X. Chen, S.H. Cai, C.B. Cai, Z. Chen, High-resolution two-dimensional correlation spectroscopy in inhomogeneous fields: new application of intermolecular zero-quantum coherences, *J. Chem. Phys.* 132 (2010) 134507.
- [31] K. Nagayama, A. Kumar, K. Wüthrich, R.R. Ernst, Experimental techniques of two-dimensional correlated spectroscopy, *J. Magn. Reson.* 40 (1980) (1969) 321–334.
- [32] R. Freeman, H.D.W. Hill, High-resolution study of NMR spin echoes: “ J spectra”, *J. Chem. Phys.* 54 (1971) 301–313.
- [33] W. Richter, W.S. Warren, Intermolecular multiple quantum coherences in liquids, *Concepts Magn. Reson.* 12 (2000) 396–409.
- [34] T.L. Hwang, A.J. Shaka, Water suppression that works. Excitation sculpting using arbitrary wave-forms and pulsed-field gradients, *J. Magn. Reson. Ser. A* 112 (1995) 275–279.
- [35] M.L. Liu, X.A. Mao, C.H. Ye, H. Huang, J.K. Nicholson, J.C. Lindon, Improved WATERGATE pulse sequences for solvent suppression in NMR spectroscopy, *J. Magn. Reson.* 132 (1998) 125–129.
- [36] Y.Q. Lin, T.L. Gu, Z. Chen, S. Kennedy, M. Jacob, J.H. Zhong, High-resolution MRS in the presence of field inhomogeneity via intermolecular double-quantum coherences on a 3-T whole-body scanner, *Magn. Reson. Med.* 63 (2010) 303–311.
- [37] E.R. Jenista, R.T. Branca, W.S. Warren, Hyperpolarized carbon-carbon intermolecular multiple quantum coherences, *J. Magn. Reson.* 196 (2009) 74–77.
- [38] Y.Q. Huang, W. Zhang, S.H. Cai, J.H. Zhong, Z. Chen, Homonuclear decoupled proton NMR spectra in modest to severe inhomogeneous fields via distant dipolar interactions, *Chem. Phys. Lett.* 492 (2010) 174–178.
- [39] W. Zhang, C.B. Cai, S.H. Cai, X. Chen, Z. Chen, Intermolecular double-quantum coherence NMR spectroscopy in moderate inhomogeneous fields, *Spectrosc. Acta Part A – Mol. Biomol. Spectrosc.* 74 (2009) 1138–1144.
- [40] E. Kupce, R. Freeman, Fast multi-dimensional Hadamard spectroscopy, *J. Magn. Reson.* 163 (2003) 56–63.
- [41] E. Kupce, R. Freeman, Fast multidimensional NMR: radial sampling of evolution space, *J. Magn. Reson.* 173 (2005) 317–321.
- [42] E. Kupce, R. Freeman, Fast multi-dimensional NMR by minimal sampling, *J. Magn. Reson.* 191 (2008) 164–168.
- [43] S.J. Nelson, D.B. Vigneron, J. Star-Lack, J. Kurhanewicz, High spatial resolution and speed in MRSI, *NMR Biomed.* 10 (1997) 411–422.
- [44] M. Gu, C.L. Liu, D.M. Spielman, Parallel spectroscopic imaging reconstruction with arbitrary trajectories using k -space sparse matrices, *Magn. Reson. Med.* 61 (2009) 267–272.
- [45] M. Lustig, D. Donoho, J.M. Pauly, Sparse MRI: the application of compressed sensing for rapid MR imaging, *Magn. Reson. Med.* 58 (2007) 1182–1195.
- [46] M. Lustig, D.L. Donoho, J.M. Santos, J.M. Pauly, Compressed sensing MRI, *IEEE Signal Process. Mag.* 25 (2008) 72–82.